# Analyst

## COMMUNICATION

Check for updates

# Measurement of the effective electric field radius on digital ion trap spectrometer†

Fuxing Xu,* Weimin Wang, (iD) ‡ Liuyu Jin, Bingjun Qian and Chuan-Fan Ding*

The effective electric field radius is a fundamental parameter of ion traps, and it has a significant influence on ion-trapping capability, signal intensity, mass range and some other properties of the ion trap. For a quadrupole ion trap built with ideal hyperbolic electrodes, its effective electric field radius can be obtained by its geometrical size, while it is very difficult to obtain the effective electric field radius for a non-hyperbolic ion trap. In this study, the effective electric field radius of a linear ion trap and some ceramic rectilinear ion traps (cRITs) were investigated *via* the digital ion trap technology. The dipole frequency of supplementary AC for excitation was locked at a certain value of the main RF trapping wave, and the characteristic $q$ values for excitation could be determined accordingly. The $q$ values could be further used to calculate the effective electric field radius through theoretical calculations. A linear equation had been fitted between the $q$ values for excitation and the square of period $T^2$ through experiments subsequently. The relative deviation between the measured electric field radius and the simulative electric field radius is less than 2%. The simulation results and experimental validation show that the approach has predictive power for modeling and measuring the effective field radius of non-hyperbolic ion traps. It is certainly significant for further understanding the performances of non-hyperbolic quadrupole systems.

## Introduction

Mass spectrometry (MS) plays an increasingly important role in chemical and biological analyses due to its wide applica-

*Key Laboratory of Advanced Mass Spectrometry and Molecular Analysis of Zhejiang Province, Institute of Mass Spectrometry, School of Materials Science & Chemical Engineering, Ningbo University, Ningbo, Zhejiang 315211, China.*
*E-mail: dingchuanfan@nbu.edu.cn, xufuxing@nbu.edu.cn; Tel: +86-0574-87605710*

†Electronic supplementary information (ESI) available: Related parameters of the digital ion trap mass spectrometer; Introduction to the simulation process with Axsim; Measurement of the effective electric field radius through experiments for cRITs with $x_0 \times y_0 = 6.50$ mm × 5.00 mm and $x_0 \times y_0 = 7.00$ mm × 5.00 mm when $q$ was fixed at 0.3522. See DOI: 10.1039/d1an00468a
‡These authors are contributed equal.

bility, as well as fast and high sensitivity and specificity. Among the different types of mass spectrometers, the ion trap (IT) mass spectrometer is used in numerous cases because of its specific characters of ion storage, multiple-stage mass-selected isolation, ion dissociation and molecular structure analysis.[1–3] The pioneer ion trap called Paul Trap is a 3D hyperbolic ion trap, which could generate an ideal quadrupole electric field. An ion trap by the application of the $U + V\cos(\Omega t)$ voltage at the ring electrode can be described by the stability diagram related to the $a$ and $q$ variables that are defined as

$$q_u = \frac{4eV}{mr^2\Omega^2} \quad (1)$$

$$a_u = -\frac{8eU}{mr^2\Omega^2} \quad (2)$$

where $m$ and $e$ are the mass and charge of ion; $U$ is the DC component of the voltage applied to the ring electrode, $V$ is the amplitude of the radio frequency (RF) voltage, and $\Omega$ is the RF frequency. $q$ and $a$ are the Mathieu parameters representing the stability of ion trajectories in the $r$- and $z$-directions, respectively, and these parameters must be within specific ranges for ion trapping. Here, $r$ is the so-called effective electric field radius of the ion trap, which measures the distance between two relative hyperbolic electrodes.[4] The effective electric field radius influences the ion trapping region, and it affects the ion cloud radius, which determines how far can ion trap miniaturization go.[5] The pseudopotential depth,[6] field distribution of multipole[7] and trapped ion number could also be calculated by obtaining the effective electric field radius. The mass range of the ion trap could be extended by decreasing the effective electric field radius when the RF voltage and frequency are fixed according to eqn (1) and (2).

Numerous evolved ion trap analyzers have been explored and fabricated during past decades, such as cylindrical ion trap (CIT), rectilinear ion trap (RIT), printed circuit board ion trap (PCBIT), mesh-electrode linear ion trap (MELIT), triangular-electrode linear ion trap (TeLIT) and halo ion trap.[8–13] For these ion traps, ions are trapped in the axial direction instead

of in the center, which benefits the trapping capacity, while the effective electric field radius of these ion trap analyzers cannot be directly calculated through the eqn (1) and (2) as they are not ideal hyperbolic electrodes.

The digital ion trap (DIT) is suited for theoretical studying and miniaturization and has been used to reduce the chemical mass shifts[14] and detecting biological molecules.[15] The ion trapping field and excitation electric field in DIT were provided by switching voltages. The timings of these switching circuits are controlled by high-precision digital circuits. It is normally the frequency rather than the amplitude of the driving voltage that is scanned during a mass scan. Compared with the conventional RF resonator method, DIT has notable advantages such as analysis of higher $m/z$ ions at low RF voltages that could prevent the electrical discharge and digital asymmetric wave isolation (DAWI). Our recent research results found that highly efficient collision-induced dissociation (CID) can be realized by simply changing the duty cycle of the resonance excitation waveform and the associated frequency.[16]

In this study, the effective electric field radius of a linear ion trap and some ceramic rectilinear ion traps (cRIT) were investigated using the digital ion trap technology. The dipole frequency of supplementary AC for excitation was locked at a certain ratio value of the main RF trapping wave, and the characteristic $q$ values for excitation could be determined accordingly. The $q$ values could be further used to calculate the effective electric field radius through theoretical calculations. A linear equation had been fitted between the $q$ values for excitation and the square of period $T^2$ through experiments subsequently. For cRITs with $x_0 \times y_0$ = 5.0 mm × 5.0 mm, 5.50 mm × 5.00 mm, 6.50 mm × 5.00 mm, and 7.00 mm × 5.00 mm, their measured electric field radius are 4.89 mm, 5.15 mm, 5.79 mm and 6.10 mm, respectively. The relative deviation between the recorded electric field radius and the simulative electric field radius was less than 2%. The simulation results and experimental validation showed that the approach has the predictive power for modeling and measuring the effective field radius of non-hyperbolic ion traps. It is certainly significant for further understanding the performances of non-hyperbolic quadrupole systems.

## Experimental

### Theory of the digital ion trap technology

Balanced rectangular waveforms RF with similar amplitude but in the opposite phase were applied to the ring electrode. The dipolar frequency of supplementary AC for excitation was derived digitally by dividing down the RF frequency and coupling to the RF similar to conventional linear ion trap mode on the $x$-axis.[17] Stability conditions of the ion motion in a pure quadrupole field with digital waveforms may still be expressed in terms of the conventional Mathieu $(a, q)$,[18] as shown in eqn (3). We generally define $U$ to be the DC component and $V$ to be the average RF amplitude. In the present case where a square wave (50% duty cycle rectangular wave) is used, $U$ is the mean

value between the positive and negative voltage levels, and $V$ is the half-voltage difference between the positive and negative voltage levels. The first region of stability in the $(a, q)$ plane for a square wave looks similar to a sinusoidal waveform. In the following discussion, we will assume no DC voltage on the ring electrode for convenience. For the square wave, the $q$ value at the boundary of the first stability region was given as 0.7125, while it is 0.908 for the sinusoidal wave.[19]

The relationship between the $q$ values and $m/z$ in DIT can be expressed as follows:[20]

$$q = \frac{eV}{m\pi^2 r^2} T^2 \qquad (3)$$

Then, the effective electric field radius $r$ could be expressed as:

$$r = T\sqrt{\left(\frac{m}{e}\right)^{-1} \frac{V}{q\pi^2}} \qquad (4)$$

According to eqn (4), $r$ can only be calculated when $m/z$, $V$, period $T$ and $q$ are known. In the experiment, $m/z$ and $V$ can be pre-set, and $q$ can be deduced by eqn (5). According to the study by Ding, when the digital waveform is used to drive an ion trap within the first region of stability, the relationship between $q$ and $\beta$ can be expressed as below:[20]

$$\beta = \frac{1}{\pi}\arccos\left[\cos\left(\pi\sqrt{\frac{q_z}{2}}\right)\cos\left(\pi\sqrt{\frac{q_z}{2}}\right)\right] \qquad (5)$$

The excitation waveform may be generated by the frequency division of the trapping waveform. At a division ratio of $n$, the excitation waveform has a period $n$ times the period of the trapping waveform. $\beta$ is a stability parameter (characteristic exponent), which determines the ion oscillation frequencies. In this study, the relations among $q$, $\beta$ and $n$ were calculated using eqn (5) and (6), respectively, and they are listed in Table S1.†[17]

$$\beta = \frac{2}{n} \qquad (6)$$

During the ion ejection scan, ions are brought into resonance with the dipole AC excitation field and ejected from the trapping region in the order of their mass-to-charge ratios. In order to use a fixed $q$ value for excitation or ejection, the frequency of the AC should be scanned together with the primary trapping frequency RF. Also, the secular frequency $\omega_s$ of ions can be expressed in terms of the $\beta$ parameters as follows:

$$\omega_s = \frac{\beta\Omega}{2} \qquad (7)$$

### Determining the RF frequency and dipole AC frequency through fragmentation efficiency

CID (collision-induced dissociation) is usually realized when the dipole AC frequency matches the secular frequency $\omega_s$. AC is a supplementary potential coupled to the primary radio frequency, and the ion resonates excitedly and absorbs energy

from the electric field when the frequency of AC equals the secular frequency of the selected precursor ion, which would increase its kinetic energy dramatically. Collisions of the ion with the buffer gas such as helium, nitrogen or argon will convert the kinetic energy into ion internal energy. Also, eventually, the ions with high internal energy will overcome the chemical bond energy barriers and dissociate into fragments. The ion resonance excitation frequency was found through experiments by observing the CID mass spectrum. The fragmental ion with the highest fragmentation efficiency should correspond to the "right" frequency of AC.[17]

In order to use a fixed ejection $q$ value, the frequency of the supplementary AC should be scanned together with the primary trapping frequency. The supplementary AC potential is divided from the main RF power supply, and therefore, the RF frequency can also be obtained when the ion CID process is found in the experiment.

### Instrumentation

All experiments were performed on a homemade three-stage differential vacuum pumping ion trap mass spectrometry system, as previously described.[21] An electrospray ionization (ESI) source was used to produce a positive sample ion from its solution. A linear ion trap (LIT) with hyperbolic electrodes ($x_0 \times y_0 = 4$ mm $\times$ 4 mm) was placed in the third vacuum chamber to perform mass analysis, as depicted in Fig. 1a. Several gold-plated ceramic-based rectilinear ion traps (cRITs)[21] with rectangular cross-section of $x_0 \times y_0 = 5.00$ mm $\times$ 5.00 mm, 5.50 mm $\times$ 5.00 mm, 6.50 mm $\times$ 5.00 mm, and 7.00 mm $\times$ 5.00 mm, were used for further testing, and one of them is depicted in Fig. 1b. The pressure was kept at $1.0 \times 10^{-5}$ Torr for mass analysis and $8.0 \times 10^{-5}$ Torr for CID experiments. A channeltron electron multiplier (CEM 4879, Burle/Photonis, USA) was used as an ion detector. The schematic of

a whole digital ion trap mass spectrometer is presented in Fig. 1c.

Operation parameters of the digital ion trap mass spectrometer are presented in Table S2.† The ion trap operation mode consists of the following six steps:[22] (i) injection, (ii) cooling, (iii) DAWI, (iv) CID, (v) mass analysis and (vi) emptying. At the injection stage, the voltage of the front ion gate is lowered, and the ions from the ionization cell are transferred through the static lens and enter the linear ion trap. After the cooling stage (10–100 ms), the precursor ions were isolated by the digital asymmetric waveform isolation (DAWI) method.[23] Then, the ions are resonated excitedly by introducing collision gas. Finally, the ions are scanned out of the trap by resonance ejection and detected by a continuous dynode electron multiplier. The amplitude of the digital dipole waveform may be adjusted, and the dipole frequency was locked at a certain value of the main trapping wave frequency. The resonance excitation and ejection take place on which $q$ values are listed in Table S1.†

### Sample preparation

Reserpine was purchased from Aladdin-Reagent Ltd (Shanghai, China), and its solution was prepared by dissolving raw reagents with methanol/water (50 : 50 V/V, 0.5% acetic acid) into $5 \times 10^{-5}$ mol L$^{-1}$. In the experiments, the solution was pumped into an ESI capillary with an i.d. of 100 μm (TSP100200, Polymicro Technologies, L.L.C., Phoenix, AZ, USA) with a syringe pump (SP100i, World Precision Instruments, Inc., Sarasota, FL, USA.) at 1 μL min$^{-1}$.

## Results and discussion

### The measurement of the effective electric field radius of a linear ion trap

A hyperbolic electrode linear ion trap was built, and its effective electric field radius was measured first for method validation. It is constructed with four 50 mm long stainless-steel hyperbolic electrodes with $x_0 = y_0 = 4.0$ mm, and as $y_0$ represents the distance from the center to the $y$-electrodes and $x_0$ is the distance from the center to the $x$-electrodes, then its theoretic geometrical electric field radius should be $r = 4.0$ mm. According to the above discussion and eqn (5), for a given $m/z$ ion, when a resonance excitation point $q$ is selected, the optimum RF and the associated resonance frequency of AC can be found by calculating the fragmentation efficiency. To obtain the maximum fragmentation efficiency, it is necessary to measure the intensity of the precursor and fragment ions. The fragmentation efficiency was calculated using the following formula:[24]

$$\%\text{Frag eff} = \frac{\text{Maximum intensity of fragment}}{\text{Intensity of precuresor}} \quad (8)$$

In this experiment, the CID experimental mass spectrometry results at each $q$ value and the obtained optimum trapping waveform RF are shown in Fig. 2. Fig. 2a shows the isolated precursor $m/z = 609$ ions through the DAWI method,
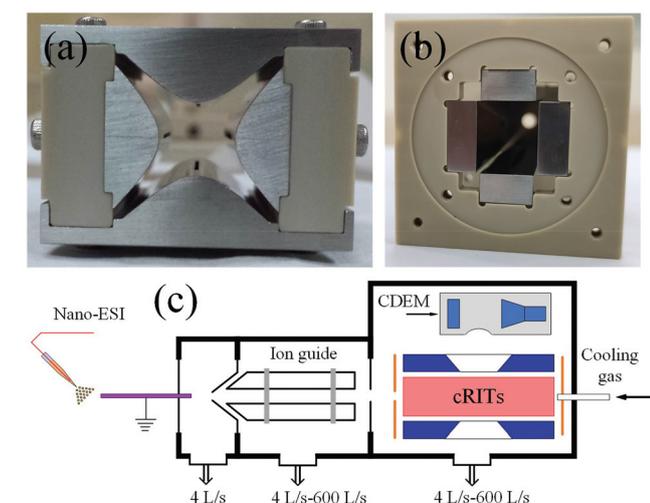


Fig. 1 (a) Photograph of the hyperbolic linear ion trap, (b) photograph of the ceramic-based rectilinear ion trap, and (c) the schematic of the digital ion trap mass spectrometer.
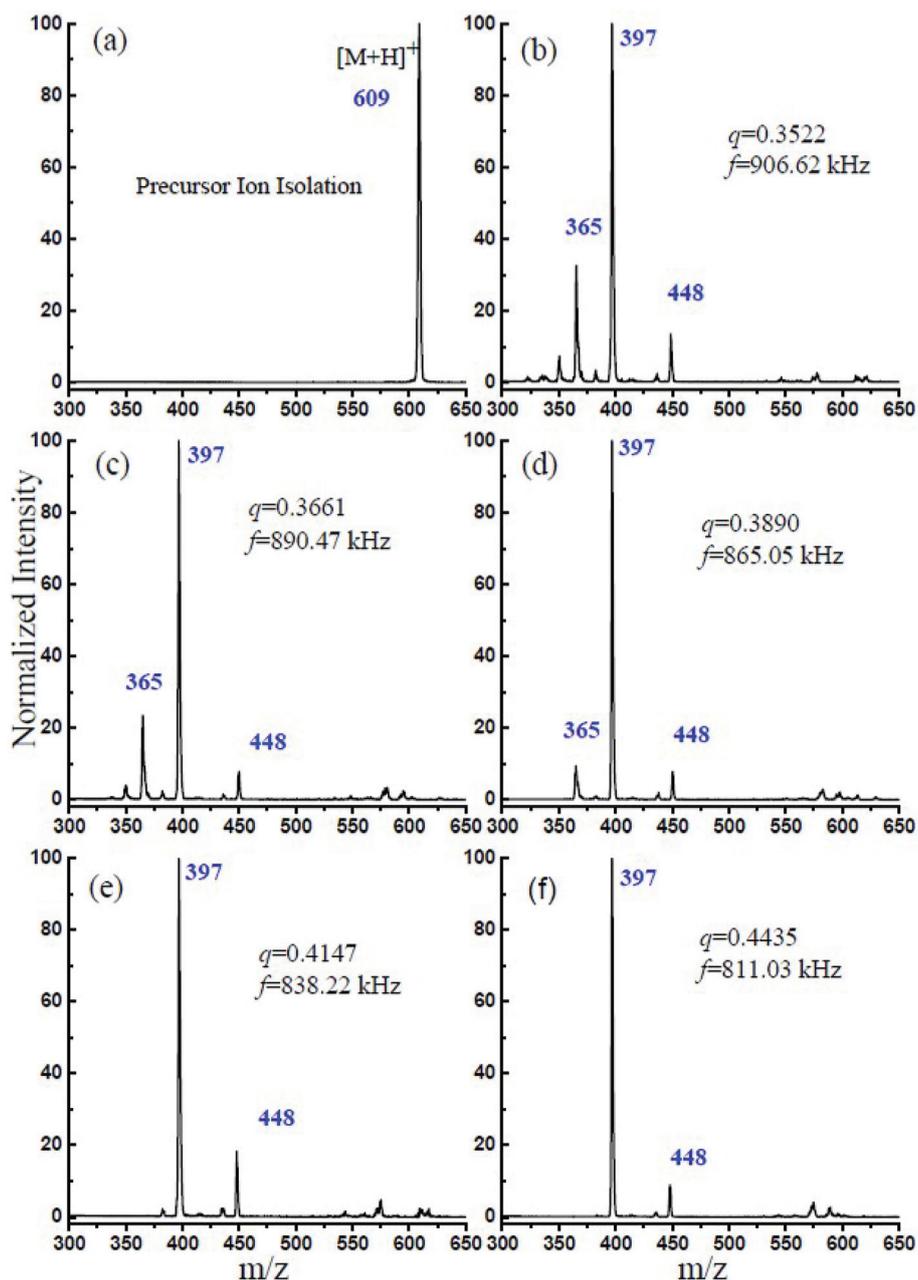
**Fig. 2** (a) Isolation of the precursor ion of reserpine $m/z$ 609. (b–f) The optimum trapping waveform frequency at different $q$ values for maximum CID efficiency.
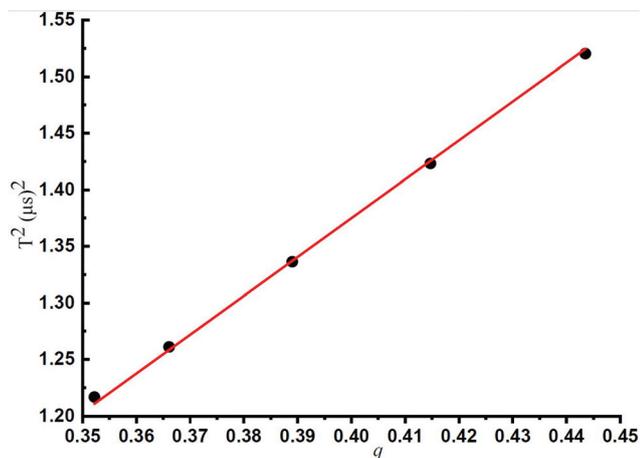
and Fig. 2b–f shows the CID results at different $q$ values and optimized RF. It was found that, for $m/z = 609$ reserpine ions, the maximum fragmentation efficiencies were obtained at 906.62 kHz, 890.47 kHz, 865.05 kHz, 838.22 kHz, and 811.03 kHz when the corresponding $q$ values were at 0.3522, 0.3661, 0.3890, 0.4147, and 0.4435. The $m/z = 448$ $[M - C_{10}NOH_{10}]^+$, 397 $[M - C_{10}O_5H_{11}]^+$ and 365 $[M - C_{10}O_5H_{11} - CH_3O]^+$ are the series of fragments from the isolated precursor ion, which had been introduced by Collings.[25] Table 1 lists the optimum trapping waveform frequencies at different $q$ values and corresponding fragmentation efficiency. The list shows that the pre-

cursor ions almost dissociated through resonance excitation at this trapping frequency of RF because the fragmentation efficiency was close to 100% gradually. It was also interesting to find that the fragmentation efficiency was increasing with the $q$ value, and the reason might be that the fragmentation is dependent on $q$.[24] The secular frequency is dependent on $\beta$, which is a function of $q$, and it is expected based upon an examination of eqn (5), indicating that increasing the secular frequency benefitted the resonance excitation.[25]

Fig. 3 shows the linear relationship between $q$ and $f$, which has been illustrated in Table 1. Under the same experimental

**Table 1** Relationship between $q$ and $f$ at optimum CID efficiency

| $q$ | $f$ (kHz) | $T$ (µs) | $1/f^2$ (µs)$^2$ | Fragmentation efficiency ($m = 397/m = 609$) × 100% |
|---|---|---|---|---|
| 0.3522 | 906.62 | 1.102 | 1.2166 | 74.25% |
| 0.3661 | 890.47 | 1.123 | 1.2611 | 78.66% |
| 0.3890 | 865.05 | 1.156 | 1.3363 | 85.66% |
| 0.4147 | 838.22 | 1.193 | 1.4232 | 88.05% |
| 0.4435 | 811.03 | 1.233 | 1.5203 | 90.22% |

conditions, the lower the $q$ values, the higher the trapping waveform frequency. A linear relationship between $q$ and the square of $T$ $(1/f^2 = T^2)$ was observed according to the experimental results, and this is very consistent with the theoretical prediction by eqn (3). The least-squares best-fit linear curve was obtained with Table 1 data subsequently. It could be deduced that for any mass-selected ion in this ion trap using DIT, its optimum trapping waveform frequency $f$ for the maximum CID efficiency could be calculated at any $q$ according to eqn (9) directly.

It could also be deduced that for any mass-selected ion in this ion trap using DIT, and the effective electric field radius could be calculated according to eqn (4). In this case, the effective electric field radius of this linear ion trap could be deduced to 4.07 mm, and it is very close to the theoretical value of $r = 4.0$ mm, which is obtained by its geometric structure. Such practice is better than just simply using one of the geometrical measured values or directly calculating the effective electric field radius with eqn (4) because fitting to multiple experiment points can reduce the measurement error.

$$T^2 = \frac{1}{f^2} = 3.43732 \times q$$
$$R_{sqr} = 0.9999$$

(9)

**Measurement of the effective electric field radius of cRITs through experiments and simulation**

Several ceramic-based rectilinear ion traps (cRITs) with different geometries were built, and their effective electric field



**Fig. 3** Relationship between $q$ and trapping waveform frequency $f$.
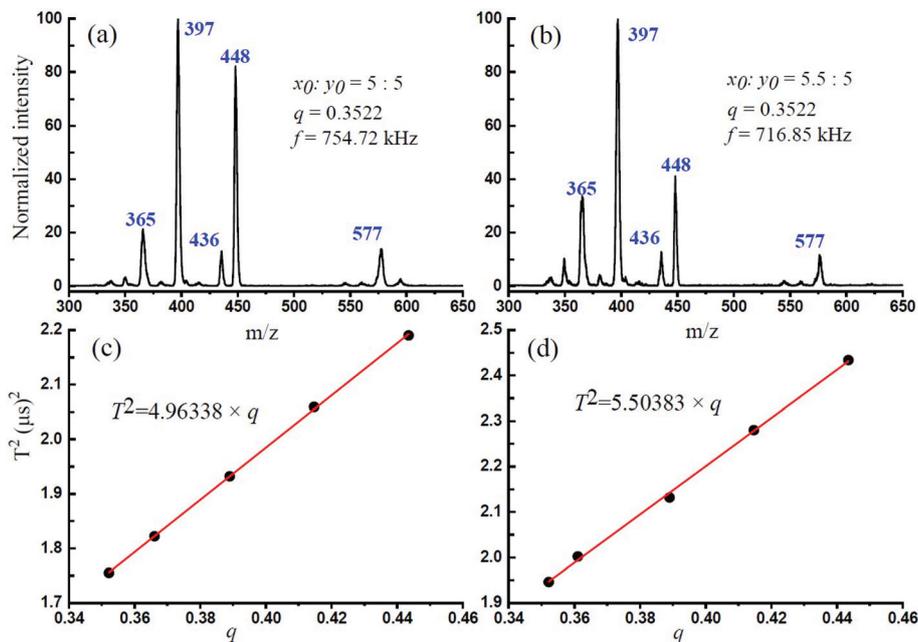


**Fig. 4** (a) The CID mass spectra of Reserpine ion ($m/z = 609$) for cRIT with $x_0 \times y_0 = 5.00$ mm × 5.00 mm when $q$ was fixed at 0.3522. (b) The CID mass spectra of the Reserpine ion ($m/z = 609$) for cRIT with $x_0 \times y_0 = 5.50$ mm × 5.00 mm when $q$ was fixed at 0.3522. (c) Relationship between $q$ and the optimum trapping waveform frequency $f$ for the maximum CID efficiency of $x_0 \times y_0 = 5.00$ mm × 5.00 mm. (d) Relationship between $q$ and the optimum trapping waveform frequency $f$ for the maximum CID efficiency of $x_0 \times y_0 = 5.50$ mm × 5.00 mm.

**Table 2**  Experimental trapping waveform frequency for CID efficiencies at different $q$ values for four cRITs

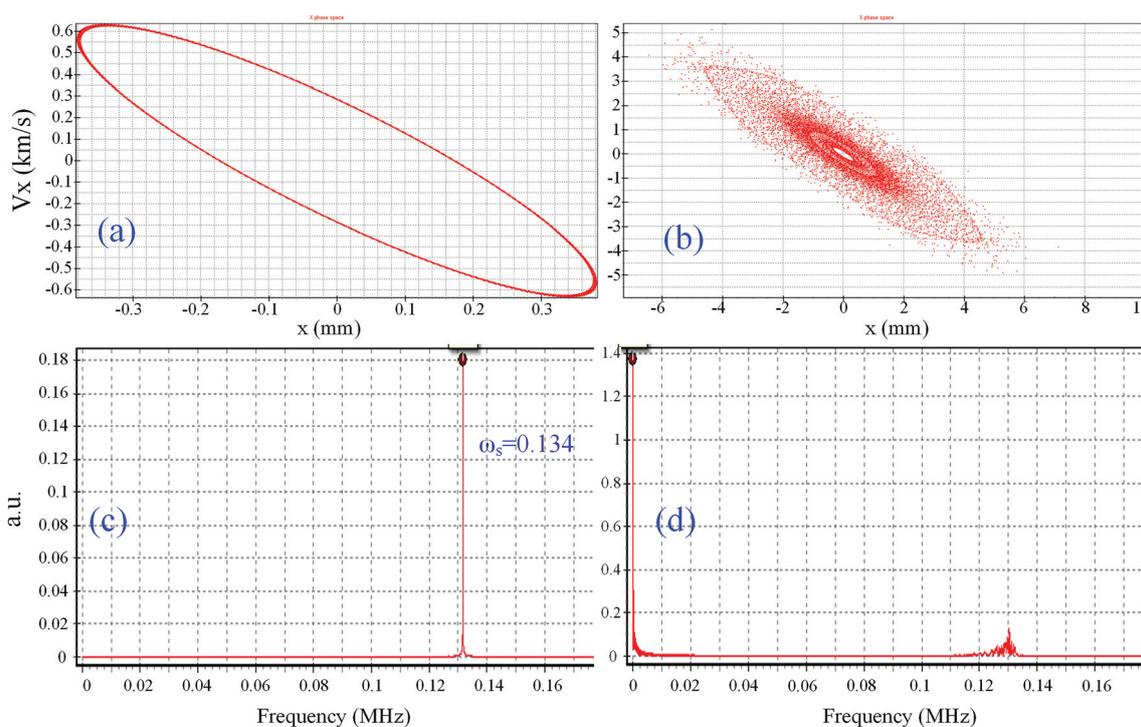| $q$ | RIT1 ($x_0:y_0 = 5:5$) | | RIT2 ($x_0:y_0 = 5.5:5$) | | RIT3 ($x_0:y_0 = 6.5:5$) | | RIT4 ($x_0:y_0 = 7:5$) | |
|---|---|---|---|---|---|---|---|---|
| | $f$ (kHz) | $T^2$ (µs)$^2$ | $f$ (kHz) | $T^2$ (µs)$^2$ | $f$ (kHz) | $T^2$ (µs)$^2$ | $f$ (kHz) | $T^2$ (µs)$^2$ |
| 0.3522 | 754.72 | 1.755 | 716.85 | 1.946 | 641.02 | 2.059 | 606.06 | 2.434 |
| 0.3661 | 740.74 | 1.822 | 706.71 | 2.002 | 626.96 | 2.148 | 591.72 | 2.544 |
| 0.3890 | 719.42 | 1.932 | 684.93 | 2.122 | 606.06 | 2.265 | 574.71 | 2.723 |
| 0.4147 | 696.86 | 2.059 | 662.25 | 2.280 | 588.24 | 2.418 | 560.22 | 2.890 |
| 0.4435 | 675.68 | 2.190 | 641.03 | 2.434 | 571.43 | 2.592 | 540.54 | 3.063 |

radius, $r$, was investigated by the above-mentioned method. The maximum fragmentation efficiencies for $x_0 \times y_0 = 5.00 \text{ mm} \times 5.00 \text{ mm}$ and $5.50 \text{ mm} \times 5.00 \text{ mm}$ were achieved, and their corresponding optimum trapping waveform frequency was at 754.72 kHz and 716.85 kHz, respectively, when $q$ was set at 0.3522. Fig. 4a and b present the experimental mass spectra results, where the precursor $m/z = 609$ ions are indis-

**Table 3**  The electric field radius through different calculation approaches

| cRIT sizes | Geometrical radius (mm) | Experimental radius (mm) | Simulative radius (mm) |
|---|---|---|---|
| cRIT1 ($x_0:y_0 = 5:5$) | 5.00 | 4.89 | 4.804 |
| cRIT2 ($x_0:y_0 = 5.5:5$) | 5.50 | 5.15 | 5.046 |
| cRIT3 ($x_0:y_0 = 6.5:5$) | 6.50 | 5.79 | 5.598 |
| cRIT4 ($x_0:y_0 = 7:5$) | 7.00 | 6.10 | 5.890 |

cernible from the background, while the main fragmental ion peaks $m/z = 448$, 397 and 365 could be found. The $m/z$ at 577 and 436 might be some tiny fragmental ions from $[\text{M} - \text{OCH}_3]^+$ and $[\text{M} - \text{C}_{11}\text{NOH}_{10}]^+$. The maximum fragmentation efficiencies for $x_0 \times y_0 = 6.50 \text{ mm} \times 5.00 \text{ mm}$ and $7.00 \text{ mm} \times 5.00 \text{ mm}$ had also been reached, and their experimental results are presented in Fig. S1† when $q$ was set at 0.3522.

Fig. 4c and d show the linear relationship between $q$ and $T^2$ for $x_0 \times y_0 = 5.0 \text{ mm} \times 5.0 \text{ mm}$ and $5.50 \text{ mm} \times 5.00 \text{ mm}$ ion trap analyzers, which are listed in Table 2. The linear equation from the least-squares best-fit could be used to calculate the optimum trapping waveform frequency $f$ for the maximum CID efficiency. Besides, for any mass-selected ion in this ion trap using DIT, the effective electric field radius can be calculated according to the above-mentioned eqn (4). In this case, the effective electric field radius of these four rectangular ion traps was 4.89, 5.15, 5.79 and 6.10 mm for $x_0 \times y_0 = 5.00 \text{ mm} \times$



**Fig. 5**  (a) The simulating $x$ phase space in the ion trap in the $x$-direction when there is no AC. (b) The simulating $x$ phase space in the ion trap on the $x$-direction when there is AC. (c) The simulative frequency spectra of reserpine in the cRIT when there is no AC. (d) The simulative frequency spectra of reserpine in the cRIT when there is AC.

5.00 mm, 5.50 mm × 5.00 mm, 6.50 mm × 5.00 mm and 7.00 mm × 5.00 mm, respectively, and it is very close to their geometrical radius.

Axsim is the software for the simulation of ion motion in dynamic mass spectrometry and was programmed by M. Sudakov,[26] and it was adopted to simulate the ion motion and spectral analysis in cRITs with different geometries. Detailed conditions of the simulation are presented in Table S3.† The secular frequency $\omega_s$ was simulated according to the experimental conditions, which means that the RF equals optimum trapping waveform frequency. $\beta$ could be deduced from eqn (7), and the $q$ values could be calculated from eqn (5). The detailed calculation process for cRITs with different sizes is presented in Tables S4–S7.†

Table 3 compares the simulated electric radius ($r_s$) with the geometrical radius ($r_0$) and the experimental results ($r_e$). It could be found that the results of $r_s$ are very close to $r_e$ and that the error was less than 2%, while the geometrical radius $r_0$ has a specific deviation with the increase in the size in the x-direction. In Fig. 5a and b, the simulative ion trajectory in the cRIT ($x_0 \times y_0$ = 5.50 mm × 5.00 mm) using the digital rectangular wave was presented, and corresponding frequency spectra to show if there is dipole AC or not proved that the resonance excitation and ejection occurred in the ion trap, where the observed $\omega_s$ = 0.134 is the secular frequency of the reserpine ion in the cRIT with $x_0 \times y_0$ = 5.50 mm × 5.00 mm, and the recorded $\omega_s$ = 0 is the simulative frequency spectra of reserpine in the cRIT when there is an AC, which means that the ions resonated excitedly immediately. It also could be found that the simulative diameter of the ion cloud was within 5.5 mm approximately.

## Conclusion

The methodfor the determination of the effective electric field radius of the non-hyperbolic ion trap was developed and validated. The field radius of several rectilinear ion traps was investigated by both experiments and simulations using the digital ion trap (DIT) technology. The mass-selected m/z ion resonated excitedly and dissociated by digital waveform, and the ion resonance excitation frequency was determined by calculating the fragmentation efficiency. Thus, the electric field radius can be deduced by the measured frequency $f$ at preselected $q$, $V$ and m/z values. The linear relation obtained in the experiment agreed with the theoretic relationship very well, and the fitted coefficient can be used to determine the electric field radius with an error of less than 2%. The simulation result and experiment validation showed that the above approach displays potential for modeling and measuring the effective field radius of non-hyperbolic ion traps.

## Author contributions

Fuxing Xu: conceptualization, experiments, methodology, investigation and writing – original draft; Weimin Wang: methodology, simulation, investigation, writing – review and editing, and resources; Jin Liuyu and Bingjun Qian: review and editing; Chuan-Fan Ding: writing – review and editing, funding acquisition and supervision.

## Conflicts of interest

The authors declare no competing financial interest.

## Acknowledgements

## References

1 Y. Wang, X. Zhang, Y. Zhai, Y. Jiang, X. Fang, M. Zhou, Y. Deng and W. Xu, *Anal. Chem.*, 2014, **86**, 10164–10170.

2 L. Li, X. Zhou, J. W. Hager and Z. Ouyang, *Anal. Chem.*, 2014, **139**, 4779–4784.

3 Z. Xu, T. Jiang, Q. Xu, Y. Zhai and W. Xu, *Anal. Chem.*, 2019, **91**, 13838–13846.

4 R. E. March, F. A. Londry and R. L. Alfred, *J. Mass Spectrom.*, 2010, **27**, 1151–1152.

5 Y. Tian, J. Higgs, A. Li, B. Barney and D. E. Austin, *J. Mass Spectrom.*, 2014, **49**, 233–240.

6 Z. Ouyang and R. G. Cooks, *Annu. Rev. Anal. Chem.*, 2009, **2**, 187–214.

7 R. E. March, *Rapid Commun. Mass Spectrom.*, 1998, **12**, 1543–1554.

8 L. S. Riter, Y. Peng, R. J. Noll, G. E. Patterson, T. Aggerholm and R. G. Cooks, *Anal. Chem.*, 2002, **74**, 6154–6162.

9 W. P. Peng, M. P. Goodwin, Z. Nie, M. Volny, Z. Ouyang and R. G. Cooks, *Anal. Chem.*, 2008, **80**, 6640–6649.

10 D. Jiang, G.-Y. Jiang, X.-X. Li, F. Xu, L. Wang, L. Ding and C.-F. Ding, *Anal. Chem.*, 2013, **85**, 6041–6046.

11 L. Wang, F. Xu, X. Dai, X. Fang and C.-F. Ding, *J. Am. Soc. Mass Spectrom.*, 2014, **25**, 548–555.

12 Y. Xiao, Z. Ding, C. Xu, X. Dai, X. Fang and C.-F. Ding, *Anal. Chem.*, 2014, **86**, 5733–5739.

13 M. Wang, H. E. Quist, B. J. Hansen, Y. Peng, Z. Zhang, A. R. Hawkins, A. L. Rockwood, D. E. Austin and M. L. Lee, *J. Am. Soc. Mass Spectrom.*, 2011, **22**, 369–378.

14 L. Sun, B. Xue, Z. Huang, P. Cheng and L. Ma, *J. Am. Soc. Mass Spectrom.*, 2018, **29**, 1386–1393.

15 K. W. Lee, C. P. Harrilal, L. Fu, G. S. Eakins and S. A. Mcluckey, *Int. J. Mass Spectrom.*, 2020, **458**, 116437.

16 F. Xu, C. Xu, L. Ding, M. Zhou and C.-F. Ding, *Int. J. Mass Spectrom.*, 2018, **428**, 29–34.

17 F. Xu, Q. Dang, X. Dai, X. Fang, Y. Wang, L. Ding and C.-F. Ding, *J. Am. Soc. Mass Spectrom.*, 2016, **27**, 1351–1356.

18 N. V. Konenkov, M. Sudakov and D. J. Douglas, *J. Am. Soc. Mass Spectrom.*, 2002, **13**, 597–613.

19 A. Berton, P. Traldi, L. Ding and F. L. Brancia, *J. Am. Soc. Mass Spectrom.*, 2008, **19**, 620–625.

20 L. Ding, M. Sudakov, F. L. Brancia, R. Giles and S. Kumashiro, *J. Mass Spectrom.*, 2004, **39**, 471–484.

21 L. Wang, F. Xu and C.-F. Ding, *Rapid Commun. Mass Spectrom.*, 2012, **26**, 2068–2074.

22 F. Xu, L. Wang, X. Dai, X. Fang and C.-F. Ding, *J. Am. Soc. Mass Spectrom.*, 2014, **25**, 556–562.

23 F. L. Brancia, B. Mccullough, A. Entwistle, J. G. Grossmann and L. Ding, *J. Am. Soc. Mass Spectrom.*, 2010, **21**, 1530–1533.

24 B. A. Collings, *J. Am. Soc. Mass Spectrom.*, 2007, **18**, 1459–1466.

25 B. A. Collings, W. R. Stott and F. A. Londry, *J. Am. Soc. Mass Spectrom.*, 2003, **14**, 622–634.

26 M. Sudakov, *User's Manual Version 2010*, St. Petersburg, 2010.